

The Australian DEBASS Survey Two Years in: Measuring the Quality and Utility of Low-Redshift Type Ia Supernova Samples

Olivia H. R. Walters and Brad E. Tucker

14 June 2023

ABSTRACT

The Dark Energy Bedrock All Sky Survey (DEBASS) is a three-year program to observe low-redshift type Ia supernovae (SNe Ia). The Australian branch acts as a spectroscopic compliment to the whole of the project for the purposes of classifying observed transients and SNe Ia model training. This report aims to analyse the current progress being made on the Australian DEBASS survey; the size of the data set, the progress that has been made, the redshift range covered, and the signal-to-noise ratio. The report focuses on the use-cases of SNe Ia, notwithstanding its use for future dark energy calculation and model training, but including the investigation of metallicity, subclassing, phase, etc. The report uses classification tools such as Supernova ID (SNID), SuperFit (SF), and DASH to analyse the survey data. As of the 23rd of February 2023, the data has a mean and median signal-to-noise ratio of 11.6 and 6.2 when looking at the R-band respectively. At least half the survey is not fit for the secondary goal of spectral analysis. From the classification tools, an estimated 60% of the survey is SNe Ia; 45 SNe Ia have been observed. There is clear agreement between SF, SNID, and human analysis, with SF proving the most reliable. SF has a K-S agreement with a uniform distribution corresponding to a $p = 0.0797$ confidence i.e. SF is approximately uniform. For $z < 0.08$ SF and SNID strongly agree with each other to $p = 0.9624$ confidence. This distribution implies the survey is fit for its primary goal of distance estimation.

1 INTRODUCTION

The nature of dark energy is a defining problem in cosmology. The ongoing attempts to measure the parameters of the dark energy equation of state is a fundamental to understanding the nature of the universe. Cosmologists not only require a consistent tool to reliably measure the dark energy parameter, but also for the broader purpose of distance estimation; being able to use standard candles in the cosmic distance ladder.

Type Ia supernovae (SNe Ia) have been a useful tool in cosmology for these purposes. This is seen in the Dark Energy Survey (DES) (Macaulay et al., 2019), the SDSS-II and SNLS surveys (Betoule et al., 2014), and the Foundation Supernova Survey (Foley et al., 2017). Further historical examples include the initial discoveries and conceptual development thereof Filippenko & Riess (1999); Riess et al. (1998); Perlmutter et al. (1999). The unique properties of SNe Ia provide an understanding of why they are so reliable to distance estimation, due to how long it takes for the SN Ia to rise to a maximum brightness (Coelho et al., 2014). Over the years, model fitting for SNe Ia light curves has become important due to the utility of having a high-luminosity standard distance measure; programs such as SALT2 combine both light curves and spectra to provide more accurate distance estimates (Guy et al., 2007; Taylor et al., 2021).

However, light curve analysis in more recent years has shown limitations. Light curves cannot account for the different subclasses of Type Ia supernova, nor their progenitor system (Ruiter, 2019; Coelho et al., 2014). Furthermore, there may be several other confounding variables that affect the shapes and phases of SNe Ia light curves that require spectral analysis to account for: metallicity, host galaxy environment, phase, etc. These several confounding variables will

be investigated throughout the report. These confounding variables make it harder to establish a simple correlation between the shape of a light curve and distance, resulting in less reliability and validity in the use of SNe Ia for distance estimation.

There is an additional lack of SNe Ia in the low-redshift range, as many SNe Ia were observed pre-digitally. More data is required in order to strengthen the models currently used to determine the properties of SNe Ia, and to gain better estimates of the cosmological constant. This is especially important given that, even with the results of the Dark Energy Survey, there are still large uncertainties in the measurements of the dark energy equation of state parameter, w , and the Hubble parameter, H_0 (di Valentino et al., 2021; Macaulay et al., 2019). More to the point these quantifiers of universal expansion rate differ between different distance estimators (di Valentino et al., 2021). Suffice it to say: more data is required, including that of SNe Ia.

Obtaining a spectrum in the optical range of a SN Ia can provide insight into these confounding variables and inform a surveyor of the parameters that may affect the distance estimate of an SNe Ia. SALT2 is an exemplary program that allows researchers to better measure light curve properties (Guy et al., 2007). Spectral analysis is also generally useful for pointing out variations in SNe Ia, which can be a precursor to analysis of progenitor systems, among many other potential use-cases (Coelho et al., 2014).

The DEBASS survey acts as a low-redshift precursor to the Legacy Survey of Space and Time (LSST) which provides a low-redshift bedrock for the LSST's focus on higher redshift lookback times (Gris et al., 2023). Much like this report, researchers working with the LSST have also considered the potential roadblocks to creating a robust dataset of SNe Ia and the utility of the collected data

([Nicolas et al., 2021](#)) in addition to how other branching projects, like the Euclid mission, can be incorporated with the LSST ([Bailey et al., 2022](#)). Low-redshift supernovae are additionally less likely to experience lensing effects caused by a non-homogeneous space time, meaning that it can aid further in measuring the curvature of space-time ([Shah et al., 2023](#)).

There are several aspects to consider when attempting to make reasoned judgements on the progress of the DEBASS survey. Outlined in this report are three separate key areas of focus, each concerning their own statistical and qualitative analyses.

Quantity, (see Section [2.3](#)) refers to the size of the data set, how much of the desired SNe Ia have been observed, and the variety in redshift range the survey covers. Ideally, a uniform distribution of SNe Ia across a redshift range of $0 < z < 0.15$, or at least uniform within the range $0 < z < 0.08$ is desired. This would make the resultant data set useful in the survey's primary task: measuring the dark energy equation of state using a Hubble Diagram.

The current limitations to measuring the dark energy equation of state include a lack of a low-redshift accuracy anchor that provides more confidence in the fit ([Kelsey et al., 2020](#); [Verde et al., 2017](#); [Kim et al., 2015](#)). By focusing efforts on nearby SNe Ia, DEBASS aims to cover for this lack of accuracy.

Quality, (see Section [2.2](#)) is a measure of both the accuracy and validity of the measurements made; the cleanliness of the signal and the consistency of each SNe Ia spectra. A dataset of high quality should give a high confidence in the subclass of a SN Ia with a low level of systematic errors introduced by observational interferences.

Utility, (see Section [1.1](#)) concerns the overall scope of applications that the DEBASS survey can be used for. While the primary focus is on its use in model training and dark energy calculation, there are other future directions research could take in which having a large set of SNe Ia spectra may be useful. It is primarily a byproduct of the quantity and quality with a given focus on future research.

1.1 Utility

The primary goal of DEBASS is for both future model training and estimation of the dark energy equation of state. These two objectives are tackled by a dataset of high quality and quantity. However, it is always useful to consider the different ways in which a dataset of low-redshift supernova could be used for future research. This aspect, understanding the 'utility' of the dataset forms a secondary objective, answering the question of how this data can be used.

There are many properties of SNe Ia that require further research, most of which involve the spectral features of SNe Ia. These directions of research may become directly relevant to model training and dark energy estimation in the future as they may help inform notable caveats to how researchers can use SNe Ia as standard candles. They may also provide insight into other areas of astrophysics outside of cosmology, though this is a significantly bigger-picture view.

Metallicity and the presence of other elements can only be reliably quantified above a certain bar of signal-to-noise. For the SNe Ia with enough spectral clarity, the survey can provide data for the continued analysis of SNe Ia properties and subtypes. This report aims to use the quality of the data to assess the efficacy of the observed spectra in determining the composition of SNe Ia. Finding the actual elemental composition of each SNe Ia is beyond the scope of the report.

1.1.1 Subclasses and Progenitor Systems

The different types of subclasses inform the quality of the survey. Being able to detect and account for variations in the spectral features

of SNe Ia is not only a useful research direction, but also provides insight into how well data is being recorded and is important to gather when DEBASS eventually combines with other surveys.

While a majority of SNe Ia are "branch-normal", there exists a sizeable subset of SNe Ia that do not follow the standard spectral and light-curve features. Each spectral classification tool outlined in Section [2.4](#) will use pre-existing data banks to categorise SNe Ia based on their spectral features. The presence of Silicon in SNe Ia will be an important data point used to classify the object ([Parrent et al., 2014](#); [Meng et al., 2023](#)). The presence of other metal elements such as Ti and Ca can help determine the specific progenitor origins such as in double detonation SNe Ia or determining the detonation mass of SNe Ia ([Miles et al., 2016](#); [Zenati et al., 2023](#); [Wilk et al., 2020](#); [Collins et al., 2022](#)). As already mentioned, the presence of helium (for helium shell detonations) and hydrogen (for Ia-CSM SNe) can provide information on the progenitor system ([Liu et al., 2022](#); [Sharma et al., 2023](#)). The report by ([Maeda & Kawabata, 2022](#)) shows a specific example concerning the possible presence of OI lines in the Iax subtype.

SNe Ia spectra are also important in determining progenitor systems, which closely relate to the spectral subtype of SNe Ia. Distinctions are generally made between Sub-Chandrasekhar and Chandrasekhar mass detonations, of which the primary differences can be found in the metallicity of a SNe Ia ([Acharova et al., 2022](#); [Miles et al., 2016](#); [Bravo et al., 2022](#)).

1.1.2 Metallicity

Metallicity plays a role in the evolution of SNe Ia, particularly with an inverse relation to their efficiency ([Ruiter, 2019](#)). Iron-enrichment is a notable example of this. A report by [Gandhi et al. \(2022\)](#) showed that the "primary effect of boosting supernova Ia rates is to lower [Mg/Fe]" or other $[\alpha/\text{Fe}]$ metallicities. This report also discusses a lack of accountability on $[\text{Fe}/\text{H}]$ in low-mass galaxies, a point of further analysis being recommended. Measuring the metallicity of SNe Ia also aids in determining the progenitor of a SNe Ia. Increasing metallicity correlates with a decrease in Calcium-40, but an increase in Iron-54 and Titanium ([Miles et al., 2016](#)). The presence of Calcium also can differentiate between sub-Chandrasekhar and Chandrasekhar-mass SNe Ia, primarily from the presence or lack of a CaII doublet at 7291 and 7324 Å ([Wilk et al., 2020](#)).

This relationship also implies that metallicity may influence distance estimation of SNe Ia. Hubble residuals and age have a dependence on metallicity, which may affect the formation of an accurate Hubble diagram if left unaccounted ([Millán-Irigoyen et al., 2022](#)). This is most likely due to the effect metallicity has on the light curve evolution of SNe Ia ([Ruiter, 2019](#)).

1.1.3 Galactic Host Environment

The host environment of a SN Ia will greatly inform both the observation and formation of the supernova. In order to independently correlate redshift to distance, using the host galaxy's spectral features can provide information on redshift that does not depend on phase.

Following from [1.1.2](#), there is already an important consideration to make following the host galaxy environment in the form of the metallicity of the progenitor system. This section mentioned that there is a potential relationship on $[\text{Fe}/\text{H}]$ rates and host galaxy mass ([Gandhi et al., 2022](#)). This implies a potential dependency on environment and distance estimation.

A more direct correlation between the properties of light curves

and host galaxy environments have also been found in mass. SNe Ia located in galaxy clusters will decline over time at a rate faster than in the field, and furthermore these clusters are generally found in higher-mass environments (Toy et al., 2023). Higher mass host galaxies additionally produce brighter SNe Ia than in their lower mass counterparts (Kelsey et al., 2020). Given a relationship between mass and brightness, it is important to account for this when developing distance estimation models as obtaining peak luminosity makes up the primary component of the process. There also exists evidence that ejecta velocities from SNe Ia differ between Elliptical and Spiral galaxy types (Filippenko, 1989).

The results of DES has yielded more correlations, particularly between colour, mass step, and Hubble residuals. A 7.2σ correlation exists between the Hubble residuals and the strength of emission lines, particularly Balmer emission (Dixon et al., 2022). Often, the correlations found in the host galaxy environment depend strongly on the colour of the supernova, with more homogeneity in Hubble residuals occurring for bluer (or younger) SNe Ia (Kelsey et al., 2022). This differs from Redder objects having larger Hubble residuals (Kelsey et al., 2020). There has also been mixed evidence to demonstrate a relationship between redder SNe Ia and the host environment's colour as shown in the report by Meldorf et al. (2022), however, this conflicts with near-infrared analysis done by Johansson et al. (2021), in which no correlation was found. Thus obtaining clear R-band spectra may provide useful for research in these areas.

1.1.4 Phase

The phase of an SNe Ia is core to distance estimation as if one knows the age of the supernova and the dilation of the light curve, then they can find the point at which peak brightness occurs. From spectral analysis, the primary way in which phase can be measured is via the strength of Nickel-56 and colour. Nickel-56 is a common byproduct of SNe Ia, an element which decays into Cobalt-56 with a half-life of 6.1 days (Wells et al., 1963). By determining the strength of Ni-56, it is possible to determine the age of a SN Ia, assuming a standardised amount of initial Ni-56 (Filippenko, 1997; Parrent et al., 2014). A spectral signature at 3890 Å should be detectable and caused by multiple NiII lines occurring between 3950 and 4100 Å (Chen et al., 2022). The colour of an SNe Ia is also an indicator of age, as generally B-V changes as a function of time, where bluer SNe Ia are generally considered older (Hoeflich et al., 2017).

1.1.5 Further Spectral Analysis

There are other opportunities for spectral analysis that can be performed, some of which may indicate information on SNe Ia, their progenitors, or host galaxy environment. It is important to consider these spectral features when analysing SNe Ia. And hence, being able to find the elemental composition of each object may help in their classification or future research.

There exists a correlation between age and other spectral features in SNe Ia spectra, primarily Oxygen, Calcium, Sulfur, Silicon, and Magnesium (Filippenko, 1997). Additionally certain progenitor systems, such as helium shell double detonations, show prominent TiII absorption features as well as line blanketing by CrI and FeI peaks (Collins et al., 2022). As mentioned in previous sections, there are trends that relate host galaxy lines, specifically [OII] (4.4σ) and the Balmer series (3σ), to Hubble residuals (Dixon et al., 2022). Of course, it is important to differentiate SNe Ia from other types of supernovae. Several statistical models have been developed to eliminate these, but outside of the use of strong SiII lines and a lack of

neutral Hydrogen in the spectra, there could be more ways to photometrically eliminate contaminants from a sample (Vincenzi et al., 2022; Filippenko, 1997).

2 METHODOLOGY

Several points of analysis were conducted on the existing 75 SNe Ia candidates, all of which were retrieved from the DEBASS database on the 24th of February 2023. Each component of the methodology aimed to investigate different aspects of the SNe Ia, ranging from the quantity, quality, and utility of the dataset.

2.1 Observation & WiFeS

All SNe Ia were observed using the Australian National University (ANU) 2.3m telescope for data consistency. An added benefit of using this telescope is its integration with the Wide Field Spectrograph (WiFeS), which uses integral field spectroscopy and a concentric image-slicer design to obtain a uniform image quality and wavelength per pixel for a wide field (Dopita et al., 2007). Each objects' spectra were recorded using WiFeS and condensed in python to obtain a 1-dimensional optical spectrum with corresponding uncertainty, in the B and R bands. The background dark was removed at this stage.

2.2 Quality

There are additional sources of interference in recording accurate survey data, of which needs to be accounted for; important considerations to make that may affect the validity of the overall data set. Classically, the signal-to-noise ratio of each supernovae is part of what determines the certainty in spectroscopic features. But more to this is the confidence in fitting each SNe Ia to pre-determined subtypes and spectral features when involving chi-squared analysis. Due to this, quality primarily spurs on from quantity, and one cannot be done without the other.

2.2.1 Noise

The first point of analysis is to measure the signal-to-noise ratio (SNR) of each object, to make a judgement on the quality of the dataset. The SNR per wavelength for each spectrum was calculated and then averaged (using both mean and median) to produce a SNR for each spectrum. Once this set of data was obtained, simple measurements on the mean and median of the entire set could be determined.

There are several confounding variables that affect the resolution of a spectra and the confidence of the appearance of spectral lines. SNR is the most basic and best method of estimating a minimum level at which spectral analysis can be conducted. Due to these confounding variables, there is no directly quantifiable relationship between confidence in result and SNR. Instead, more arbitrary boundaries are set on what can be analysed, with the use of computer classification tools to handle the complexities of the spectra.

The most important two elements that need to be identified directly are Silicon (SiII) and Nickel (NiII) to both: determine if the candidate object is a SNe Ia; and to determine the age of the SNe Ia. These two elements fortunately have very broad and visible lines within the B and R-band ranges, meaning that a SNR of 10 is ideal for analysis with a minimum requirement of 5.

Other elements present in the SNe Ia are less crucial to the main

focus of the survey, and aim to serve the secondary goals related to classification, metallicity, etc. The best benchmark for spectral analysis on these properties is [Fe/H] metallicity, which requires a minimum SNR of 10 and an ideal SNR of 20. Other metal elements such as Titanium, Calcium, etc. and non-metal elements such as Oxygen and Helium can, for the sake of the report, only be confidently be looked at under these intervals and conditions.

2.3 Quantity

The primary goal of the Australian DEBASS project is focused on providing a follow-up on the optical-range spectra of SNe Ia analysed by the photometric part of the larger DEBASS project. The project has a goal of obtaining the spectra of 300 SNe Ia for the whole of DEBASS, the contribution targeted by the Australian National University is of at least 30 of these spectra per quarter.

Core-collapse SNe (CC SNe) are distinct from SNe Ia in their spectral features. However, there is minor overlap between SNe Ia and CC SNe such as types Ib and Ic (Filippenko, 1997). The primary spectral similarity is the common lack of hydrogen. Statistical tools are employed such as PSBEAMS in preventing these CC SNe from contaminating a dataset, see Foley et al. (2017) as an example of its use. However, it is best to eliminate CC SNe photometrically before a data set is fully compiled.

What complicates this matter further is that several subclasses of SNe Ia share similar spectral features to CC SNe, for example the presence of HeI lines in both SNe Ib and certain subclasses of peculiar SN Ia, generated by Helium shell explosions (Liu et al., 2022; Collins et al., 2022; Filippenko, 1997).

Obtaining a diverse range of SNe Ia subtypes can provide for useful future research, however consistency is important to maintain i.e. what is measured are reliably SNe Ia. In statistical terms, the aim is to maximize the sensitivity and minimize the specificity of the collection method as early as possible.

Of course, redshift is of key importance to analysis. Having a broad range of redshift values is key for measuring the dark energy equation of state. Hence it is important to aim for as uniform of a spread as possible across the low-redshift range. Measuring uniformity may involve comparing the sample with a uniform distribution.

This closely relates to the existing statistical Kolmogorov–Smirnov test (KS-test), in which a single sample can be compared against a uniform distribution to provide a statistic on the uniformity of the redshift distribution (Smirnov, 1948). It is important to note that both methods for discrete samples will not provide a ‘perfect statistic’ unless if the sample is infinitely large, hence the statistic will need to be reduced to be viable for analysis.

A single-sample and two-sample KS-test was utilised in determining the nature of the distribution. The KS statistic for a single and two sample test is as follows:

$$d = \sup |F_n(x) - F(x)| \quad (1)$$

$$d_{n,m} = \sup |F_n(x) - F_m(x)| \quad (2)$$

Where $F_n(x)$ and $F_m(x)$ are the empirical distribution functions of the sample sets. A strong approximation (1000 term sum) of the Kolmogorov Distribution was used, the full distribution is:

$$P(K \leq x) = \frac{\sqrt{2\pi}}{x} \sum_{k=1}^{\infty} \exp\left(-\frac{(2k-1)^2\pi^2}{8x^2}\right) \quad (3)$$

From the KS-test statistic, a reduced test statistic can be generated that accounts properly for the size of the data set (i.e. is invariant with the data set size):

$$k = \sqrt{nd} \quad (4)$$

$$k_{n,m} = \frac{nm}{n+m} d_{n,m} \quad (5)$$

The p-value is determined by $p = 1 - P(K \leq k)$ with the null hypothesis being that there is no significant difference between the two distributions. This report aims to have all p-values be greater than a standard critical value of $\alpha = 0.05$ when comparing with a uniform distribution i.e. it is expected that the null hypothesis is accepted.

It is important for the validity of the report to attempt to obtain redshifts independently of distance, generally relying on the host galaxy environments instead. A circular dependency may arise between redshift and distance, resulting in poor data analysis and deduction.

2.4 Pipeline of Data Analysis

The next step involved analysing each spectra using proprietary programs: SuperFit (SF), Supernova Identification (SNID), and the Deep Automated Supernova and Host classifier (DASH) (Blondin & Tonry, 2007; Muthukrishna et al., 2019; Howell et al., 2005). Each program has a similar purpose: to classify and derive the properties of each SNe Ia using a series of preceding data bank examples.

From this analysis, the redshift, age, confidence intervals, host galaxy environment, and subtype were of primary importance. Corroboration of the three separate programs which all calculate redshift independent of light curve provided an even more precise estimation for the data points of concern. The derived and condensed data from each proprietary program was then separately analysed according to the data point in question.

2.4.1 Data Analysis

The aim of using SF was to gain insight on the host galaxy environment during the process of classifying the SNe Ia. Each SNe Ia was programmatically compared to 75 different sample objects occurring in separate host galaxy environments, each resulting in a redshift, phase, galaxy type, and band. Coupled with each comparison was a reduced Chi-squared statistic.

For each SNe Ia, the classifying list was then condensed by first taking the best five fits according to reduced chi-squared values. The mean and uncertainty in the redshifts and host galaxy parameters were recorded into a single record. A weighted modal analysis was conducted on the remaining set of five samples, prioritising the mode of the band, host galaxy, and then phase to minimise the amount of possible sample candidates for each spectra. The host galaxy modal analysis involved binning each type into three classes: Elliptical (E, S0), Spiral (Sa-Sc), and Starburst (SB1-6). It is important to note that Lenticular (S0) galaxies are generally classified as spirals under the Hubble Scheme. Further information on the specifics of the modal analysis are found in section 2.4.2.

This condensed set of samples provided a set of candidate types, confidence intervals, along with a corresponding redshift. This was further pipelined into quantifying the spread of the data.

SNID did not account for host galaxies and used a more focused approach on SNe Ia subtype. Resultant data came in the form of spectral subtypes and redshifts coupled with confidence intervals

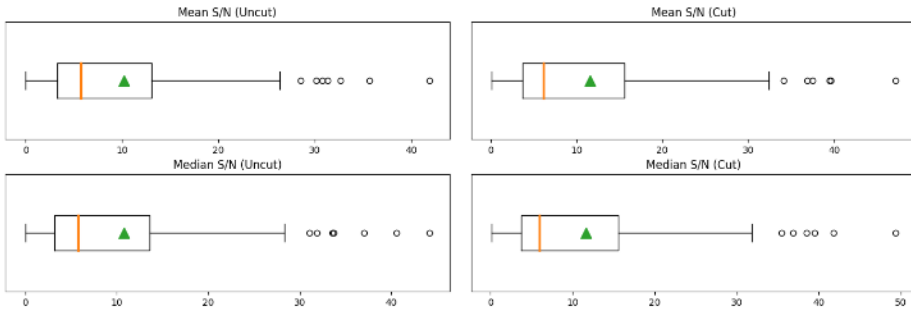


Figure 1. Boxplots displaying the mean and median signal-to-noise ratios of each object in the sample, similar to fig. 2. On the left are the boxplots of mean object signal-to-noise (top left) and median object signal-to-noise (bottom left), where the signal-to-noise ratio was calculated over the whole wavelength range of each optical spectra. On the right are boxplots of mean object signal-to-noise (top right) and median object signal-to-noise (bottom right), where the signal-to-noise ratio was calculated in the optical range of 5300 - 9000 Å.

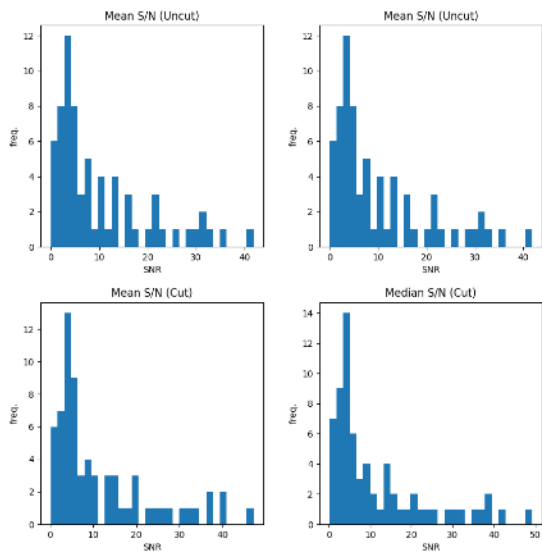


Figure 2. Histograms displaying the mean and median signal-to-noise ratios of each object in the sample, similar to fig. 1. On the left are the boxplots of mean object signal-to-noise (top left) and median object signal-to-noise (bottom left), where the signal-to-noise ratio was calculated over the whole wavelength range of each optical spectra. On the right are boxplots of mean object signal-to-noise (top right) and median object signal-to-noise (bottom right), where the signal-to-noise ratio was calculated in the optical range of 5300 - 9000 Å.

for the goodness of fit. The compiled results were then analysed in a similar fashion to SF - using a weighted mode analysis on the amount of each subtype matched by the program. The top 5 candidate type results were collated and for each of the these candidate types, a computer program would go into every model object and calculate the most likely designated type based on the rlap confidence.

DASH is the final program used in the analysis of SNe Ia. Unlike the previous two, DASH applies artificial intelligence. While DASH can classify host galaxy properties, only the candidate object was analysed using DASH. Similarly, the program does not require much model fitting, however without the presence of host galaxy properties,

it means that there may be limited analysis that can be performed by DASH.

Each SNe Ia candidate after DASH analysis would be automatically capable of returning the top 5 results. DASH additionally performs its own analysis on each of the candidate types to produce a singular set of most-likely values for age, redshift, and confidence. The post-processing conclusions decided by DASH were taken and recorded into the project's repository. DASH does not provide a chi-squared or rlap statistic, instead opting for confidence. This was taken as the given confidence value for the DASH component of classification.

The three data sets generated from each of the three programs was then used to provide an EDF of redshift and age based on SNe Ia subtype classification or just in general. Which, with applied KS-tests, can allow for a quantitative measure of the agreement between the three data sets in addition to their agreement to a uniform model. These distributions were analysed by eye additionally to point out necessary features in the expected redshift and age range.

The three data sets was also used to provide information on the proportion of the survey that contains SNe Ia, based on mutual consensus i.e. how much of each classification tool's data overlaps and agrees with each other about type Ia SNe.

2.4.2 Weighted Modal Analysis

As the weighted modal analysis was developed originally, it is of importance to document how the analysis was conducted, and the expected behaviours of the values. Appendix A provides an algorithm written in python that was used to calculate the weighted mode for a set of values and associated chi-squared statistics. It is also possible to perform the same analysis on uncertainties, rlap, or other statistics, however that changes whether each weight is divided or multiplied in the end. The weighted mode of the set may not be necessarily equal to the regular mode, as the consideration of frequency is biased with respect to each weight. Modal confidence for each data value is determined in eq. 6 below:

$$M_x = \frac{W_x}{\sum_{x_i} W_{x_i}}, \text{ where, } W_x = f_x \times \bar{\sigma}_x \quad (6)$$

Here, f_x is the frequency of the data point, $\bar{\sigma}_x$ is the average of the weighting statistics associated with the data point, W_x is the modal confidence, and M_x is the reduced modal confidence. The mode with

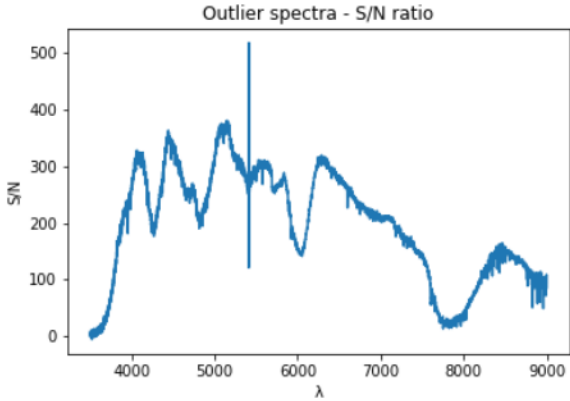


Figure 3. The signal-to-noise ratio as a function of wavelength for the spectra labelled as an outlier. This is the only object to have a mean signal-to-noise ratio 1.5 times the interquartile range, and hence is not included in the histograms in fig. 2 or the boxplots in fig. 1.

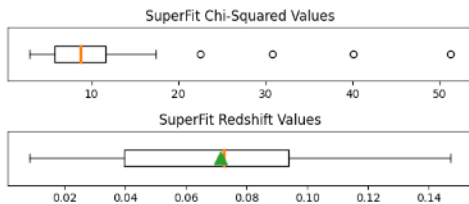


Figure 4. Boxplots of both the reduced chi-squared (top) and redshift (bottom) values obtained from the SuperFit program, following reduction using a weighted modal analysis of each candidate type.

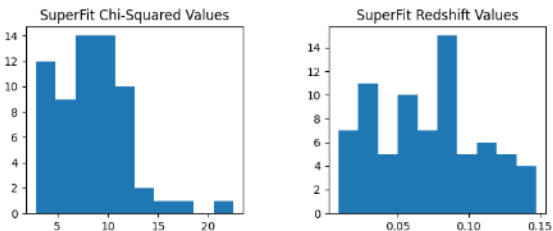


Figure 5. Histograms of both the reduced chi-squared (left) and redshift (right) values obtained from the SuperFit program, following reduction using a weighted modal analysis of each candidate type.

the highest modal confidence is the weighted mode of the data set. A reduced modal confidence was returned, which took a proportionality value from 0 to 1. If $M_x = 1$, then it implies that the dataset comprises entirely of one data point. Because of the nature of this analysis, it was possible to obtain lots of maximum confidence values, especially if a classification tool was certain of a classification.

For SF, the corresponding chi-squared statistic was used to determine the weighted mode, whereas in SNID, the RLAP was used. DASH did not require a weighted modal analysis as it performed its own data condensation.

2.5 Bias

All three programs performed calculations in a unique manner. The host galaxy environment was determined by SF, the opposite was true in the case of SNID, and DASH could do both. Using the results of two-sample KS-tests, applied to both the distributions of age and redshifts from each program, it was possible to determine if there was a bias in the different applications used by the classification tools. Biases in the observational methods could also be demonstrated by KS-tests compared against each sample. These KS-tests were performed in terms of the age and redshift distributions of the recorded SNe Ia, separated based on predicted subtype.

With the reduction of each object, human analysis was performed on each reduced spectra spectra to manually determine their subtype. A comparison between human and computational determination of subtypes was done to help highlight specific flaws in current implementations of SF, SNID, and DASH.

From Kessler et al. (2019); Foley et al. (2017), several methods of bias correction including BBC and PSBEAMS are used in conjunction with SALT2 classification tools. These corrections aim to account for the several confounding variables interfering with creating a uniform redshift distribution. Kessler et al. (2019) notes a co-moving volumetric rate following a power law of $(z+1)^2 \cdot 11$. Fig. 6 & 7 of Kessler et al. (2019) additionally provides an expected redshift distribution that is skewed towards lower z-values rather than uniform. This also applies to age, being skewed with a peak nearing zero in age.

A majority of bias correction could only be conducted after analysis of the survey. However, it is important that the report aimed for similar bias correction methods when manually analysing the redshift range of the SNe candidates to emulate the PSBEAMS model. The main proportion of bias correction conducted in the report involved mutual consensus comparison in addition to a comment being made qualitatively on the confounding factors found in the final redshift distributions.

2.5.1 Human Analysis

As data was being observed and recorded into the files for processing, human analysis was conducted on each SNe Ia candidate to provide a preliminary estimate for the type and nature of each candidate. This analysis was stored on the DEBASS website, found in the acknowledgements section. The manually conducted analysis of the spectra was used as an important, yet limited, comparison tool.

2.6 Additional Work

The compiled data and code used for analysis, along with the notes taken in order to streamline the process, was stored on a repository. The intention is to allow for future and extended analysis of the DEBASS project to be conducted without starting from scratch. The programs developed provide a detailed analysis and condensing of data, with the intent of automating the whole process from the formation of the fits files to the outputted data. While only prototypes were created, there is a base for future work to make the process of SNe Ia analysis much more streamlined and automated.

All three programs could be automatically applied using bash and python commands and it would be possible to be able to construct an algorithm that could perform a cohesive analysis on any data set. A portfolio of each individual SNe Ia candidate could be performed that displays all conclusions drawn by the computer program. The

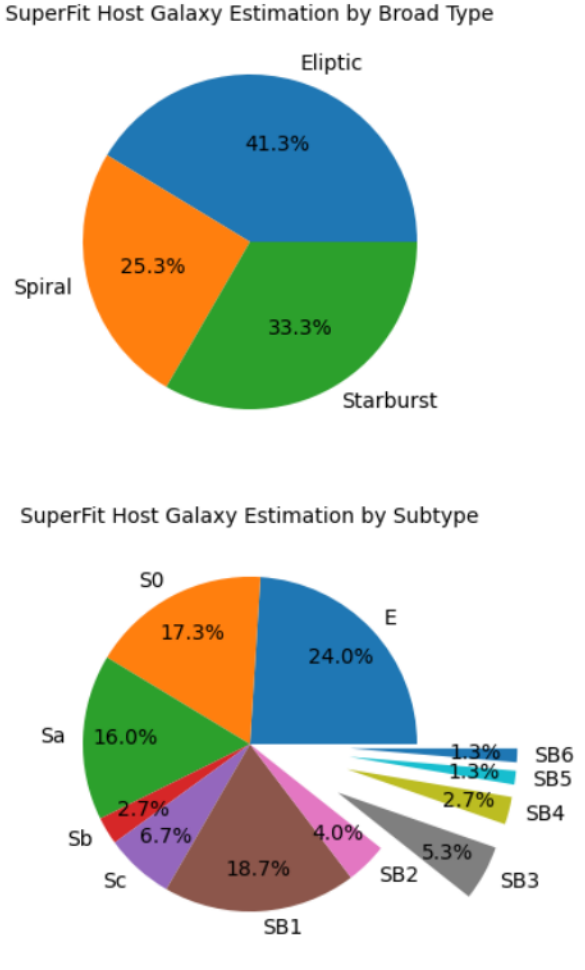


Figure 6. Two pie charts that display the host galaxy classification resultant from the SF analysis; including the classification of broad type (top) and subtype (bottom). The starburst subtypes are partly exploded for better clarity.

classification tool	Comparison CDF	k_α	p
SF	Uniform	1.269	0.0797
	Uniform	2.505	7.072×10^{-6}
SNID	Normal	0.6931	0.7227
	Uniform	2.771	4.268×10^{-7}
DASH	Normal	1.567	0.01477

Table 1. Single-sample KS-test results for each of the three classification tools when compared against a uniform distribution, including the corresponding p-values.

human analysis conducted on the website was linked to provide more information on each SNe Ia candidate object.

3 RESULTS

3.1 Signal-to-Noise Ratio

The signal to noise ratios of each object are compiled into a set of histograms and boxplots seen in figs. 2 and 1 respectively. Both the mean and median SNR for each object are calculated to ascertain

the nature of each spectra. However it appears that both measures of central tendency produce similar results i.e. there is not much of a skew in each individual object's spectra.

The uncertainty of measurement in the B-band for each object is high, and hence a series of 'cut' spectra are produced in which data points only above 5300 Å are considered, shown on the right in fig. 1. This change does not create a significant alteration to the means or medians of each object. The resultant SNR mean of means are 10.2 and 11.6 for the full and cut spectra respectively, and the SNR median of means are 5.7 and 6.2 respectively. Fig. 2 details a notable skew in the SNR values of the entire sample, indicating that a large amount of SNe Ia have very low SNR, and that a small amount has a very high SNR.

With the benchmarks of 5, 10, and 20 SNR, percentile calculation show that 60.29% of the survey is above a SNR of 5, 38.23% of the survey is above a SNR of 10, 20.59% of the survey is above a SNR of 20. The lowest value is 0.1456 and the highest value is 47.18 (excluding outliers).

The two figures exclude the SNR of one specific object, SN 2021aefx, which was excluded as an outlier. The graph of this object's SNR per wavelength is displayed in fig. 3. The reason for such a high SNR is most likely due to the proximity of the object to Earth, resulting in a significantly clearer optical spectra due to less extraneous interference. However, from this figure, the aforementioned high uncertainty in the B-Band can be seen for wavelengths below 4000 Å.

3.2 classification tools and KS-Tests

3.2.1 SuperFit

The SF analysis is discussed first. The SF model includes the highest amount of parameter modification but in return provides information on the host galaxy environment. Fig. 4 displays boxplots of the distribution of chi-squared values and redshift values. From these graphs, it is clear that most of the dataset lies in $\chi^2 < 20$, with a majority under 10. These are reduced χ^2 statistics additionally, meaning that the size of each SNe Ia candidate model is already accounted for. Fig. 5 brings more light onto the specific nature of the redshift distribution, appearing as somewhat uniform with bumps surrounding $0.08 < z < 0.09$ and $0.02 < z < 0.03$.

SF provides information on host galaxy environment, which allows the program to more cleanly determine redshift without reliance on the SNe Ia spectra. Fig. 6 displays the proportions of the dataset that SF classifies as each binned form of galaxy. As demonstrated, Elliptic galaxies are the most common to appear, followed second by starburst, with Spiral last. Elliptic galaxies are broken down in half by S0 and E subtypes, providing that only 24% of the survey are SNe Ia candidates in proper Lenticular galaxies with 17.3% being in S0. It appears that most objects are found in the early-phase spiral galaxy. This only somewhat differs from expected (Mannucci et al., 2005; Sullivan et al., 2006). "SNe Ia are more than 10 times more common in late-type, star-forming galaxies than in early-type" (Gupta, 2013).

In terms of the redshift distribution, the single-sample KS-Test is applied to compare SF with a standard uniform distribution. By eye, fig. 10 demonstrates that the SF z-distribution is nearly uniform. All of the single-sample KS statistics are displayed in table 1. A reduced KS statistic of 1.269 corresponding to a 0.9203 confidence interval is demonstrated - below the necessary critical value. The EDF of the SF redshifts, more than the histogram, demonstrate the uniformity of the distribution in the $0 < z < 0.15$ range.

classification tool	Data Point	k_α	p
SF	All z	1.715	0.005590
	$z < 0.08$	0.5022	0.9625
	Age	2.498	7.570×10^{-6}
	All z (Ia-norm only)	2.244	8.472×10^{-5}
DASH	Age (Ia-norm only)	0.5834	0.8855
	All z	1.388	0.04242
	$z < 0.08$	1.388	0.04242
	Age	2.041	0.0004807
	All z (Ia-norm only)	1.279	0.07580
	Age (Ia-norm only)	0.9381	0.3423

Table 2. Two-sample KS-test results for each of the SF and DASH classification tools when compared against SNID for various age and redshift ranges, and the subtype limitations thereof, including the corresponding p-values.

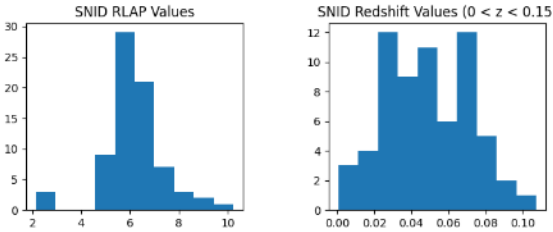


Figure 7. Histograms of both the RLAP (left) and redshift (right) values obtained from the SNID program, following reduction using a weighted modal analysis of each candidate type.

3.2.2 Supernova ID

As referenced in the method, SNID only compares from template models. Thus no host galaxy information can be classified. However, redshifts and subtype classification can still be achieved by the model. Fig. 8 highlights that SNID categorises a few candidate objects with redshifts far beyond a plausible range of $0 < z < 0.15$. These are clear outliers that SNID simply is not capable of correctly categorising rather than SNe Ia that happened to be further than thought. Hence the figure also includes a redshift-limited version of the data set, which almost entirely corrects the perceived skew in the data.

Fig. 8 also includes the errors in redshift and the RLAP values. Because there is no host galaxy classification, and that chi-squared analysis is not automatically performed by the model, it is worthwhile to ensure that the program returns consistent redshifts for each compared classification tool. e.g. determine the amount of variance in the redshifts for a Ia-norm classified SNe Ia. All redshift error values are consistently below 0.01, indicating that SNID is able to consistently classify and determine redshift. The RLAP values, a statistic desired to be maximised, also appear rather centered around 6.

The form of the redshift and RLAP values are further characterised in fig. 7, appearing by eye as normal distributions with a lack of notable skew. The redshift values also appear to have elements of uniformity to them that overlap with SF. Fig. 10 makes apparent the normal-like EDF of SNID, it also appears to demonstrate a notable lack of higher-z redshift values beyond $z = 0.08$. Taking into account the cleared outlier values, while SNID determines SNe Ia candidates to have redshifts well above $z = 0.15$, most objects determined to be in that range have values few and far between. The KS-tests in fig. 10 for SNID take into account the entire redshift range as it keeps the fit the cleanest.

Table 1 demonstrates that the SNID z-distribution has a reduced

KS statistic of 2.505 corresponding to a 7.072×10^{-6} confidence interval - well below any necessary critical value. This demonstrates that SNID is not uniform, and is more normal than anything else, shown further in fig. 12. The normal distribution used follows the mean and standard deviation of the SNID z-distribution. Table 1 states that the KS statistic using a normal CDF is 0.6931 corresponding to a 0.7227 confidence interval - which is well above any critical value.

3.2.3 DASH

Fig. 11 represents the retrieved results from DASH. Because no modal analysis is conducted on the post-processing DASH samples, less information can be directly drawn in favour of more automated classification. The DASH confidence values act in a similar light to the weighted modal analysis applied to SF and SNID. This is demonstrated in how the top box plot of fig. 11, which shows a heavy skew towards the maximum value. This is similar to how the weighted mode analysis assigns a value to 1 if all top five results are in agreement with each other.

From the boxplots in fig. 11, and even more in fig. 9, DASH's redshift values show a noticeable skew towards the lower redshift values, with a standard mode around $0.02 < z < 0.03$. There are additionally higher-z outlier values that are not included in the two figures. DASH also provides a single clear-cut range of SNe Ia candidate age, and hence it can be used as a tool for phase classification. There is a distinct skew in the lower bounds of ages for each SNe Ia candidate characterised by DASH which is not present with the upper bounds.

The skew is most apparent when performing the single sample KS-Test, which shows a large gradient in the EDF of the all-z DASH redshift distribution. In this case, all-z values are used as it cleans the fit up the best, similar to SNID. Fig. 10 shows both this skew and additionally the large gap of no data above $z = 0.08$. Because the curve only finishes at 0.75 mark, it means that 25% of the DASH classification results dictate that the redshifts are above the desired range.

Table 1 shows that DASH's z-distribution has a reduced KS statistic of 2.771 corresponding to a 4.268×10^{-7} confidence interval when compared against a uniform distribution, but a reduced KS statistic of 1.567 corresponding to a 0.01477 confidence interval when compared against a normal distribution. Similar to SNID, the DASH z-distribution is not uniform whatsoever, but fits much closer to a normal distribution as seen in fig. 12. Unlike SNID however, the corresponding p-value for a normal distribution with the same mean and standard deviation as the DASH z-distribution is low enough to conclude that DASH is not normal - expected given the heavy skew in the histograms.

3.3 Two-Sample KS-Tests

Two-sample KS-tests are also performed between the three samples. Because DASH is so different in distribution to SF, it was not considered worthwhile making a quantitative comparison as they differ too greatly. SNID, due to its qualities as similar to both SF and DASH, is used as the comparison point between the three samples. Fig. 13 shows the EDF comparison plots between the samples. SNID, despite its nature as a normal distribution, clearly matches up with SF - especially when restricting to the $z < 0.08$ range. This corresponds to larger p-values in table 2, with the $z < 0.08$ p-value demonstrating a matching correspondence. On the other hand, DASH does not appear to consistently match with SNID, in both cases having a p-value

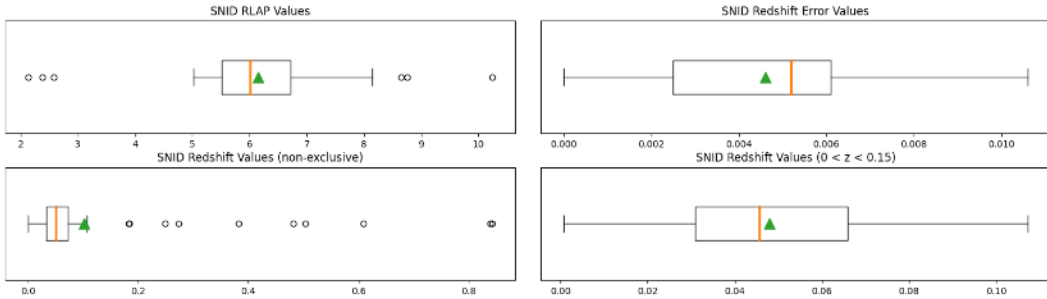


Figure 8. Boxplots of the RLAP (top), all-z redshift (middle top), $0 < z < 0.15$ redshift (middle bottom), and redshift error (bottom) values obtained from the SNID program, following reduction using a weighted modal analysis of each candidate type.

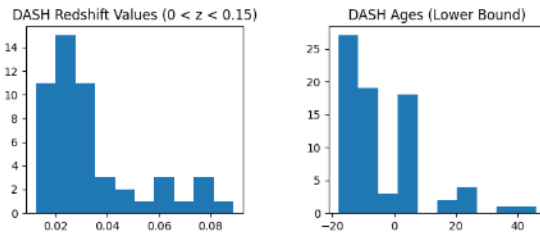


Figure 9. Histograms of the redshifts (left) and lower-bound age ranges (right) obtained from the DASH program. Some objects were found to have a redshift greater than 0.15, they are not included as they plausibly cannot be in $z > 0.15$.

of 0.04242, which is just below a standard critical value of 0.05. The likely cause of this is the skew in the DASH z-distribution shown in the figure.

It is also possible to perform two-sample KS-Tests based on the age distributions of the samples. Not enough data can be retrieved for Ia-91T, Ia-91bg, Ia-pec, and Ia-CSM. Thus only the Ia-norm or full data set can be analysed. Table 2 displays the two-sample KS statistics for age, age limited to Ia-norm SNe, and redshift limited to Ia-norm SNe. The goal of limiting to Ia-norm SNe is to further look at the quality of the data when removing subtypes that contain non-standard spectral features. The features of Ia-norm SNe are generally much more consistent than that of all subtypes of Ia SNe.

3.4 Age

Age appears as a normal distribution centred at maximum light (or zero phase), hence it is expected that all three classification tools give similarly shaped distributions. Despite this, the p-values in table 2 show that this is only the case if the data set is restricted to Ia-norm SNe Ia. Even despite this from fig. 14, SF's age distribution appears nearly uniform as well whereas SNID's is the most distinctly normal. The figure also demonstrates in the Ia-norm restricted DASH Age distribution the notable lack of Ia-norm SN candidates, appearing as a 'blocky' orange graph on the bottom right.

The age ranges displayed in fig. 14 and used in the KS analysis are determined differently for each sample. Because SF provides multiple possible age ranges, multiple different age values per object are fed into the distribution. SNID had one age value per object. DASH provided an upper and lower bound, which are averaged together to create a middle position, which potentially removes the skew in the lower bound age distribution.

3.5 Proportionality Analysis

The three classification tools are additionally utilised to determine the proportion of the survey classified as Ia-norm SNe or Ia SNe. This can further allow the report to point out biases in survey data collection or in classification approach. From table 3, SNID appears to have the highest success rate at 56 objects (74.67%), SF is midway with 45 objects (60%), and DASH is last at 35 objects (46.67%) classified as SNe Ia. When attempting to restrict this to Ia-norm SNe Ia, SNID has 50 objects (66.67%), SF has 35 objects (46.67%), and DASH has only 5 objects (6.67%). The proportions show that SNID is very likely to classify SNe Ia as Ia-norm with a sensitivity of 89.29%, SF being somewhat likely at 77.78%, and DASH being very far below both at 14.29%. It is important to note, however, that DASH is less likely to give a SNe Ia any subtype, instead marking it as simply "Ia".

In terms of non-Ia objects, DASH appears to most consistently bias itself towards other type I SNe, where more objects are determined to be SNe Ib and Ic than SNe Ia. SF appears to equally lean itself towards other type I and II SNe, whereas SNID swings more towards non-type I objects including galaxies. No distinction is made between SNe II and other non-type I SNe simply because all of them have the same presence of hydrogen that SNe I do not have, whereas the differentiating factor between Ia and Ib or Ic is the presence of Silicon and Nickel.

The manual analysis retrieves a success rate of 45 objects (60%). No overlap data could be obtained from this manual analysis. However, this data point will still provide a useful benchmark value.

It is also worthwhile to consider the overlap between the SNe classified by the different classification tools, with the aim to maximise the overlap. SF and DASH have the highest overlap with both surveys being in agreement that 41 objects (54.68%) are SNe Ia. SNID and DASH have a lower agreement with 33 objects (44%). Contrasting the KS-test redshift agreement, SNID and SF hold the lowest agreement at 26 objects (34.67%). Combining all three data sets, it is clear that the dissonance between the three surveys is mostly due to the differences in SNID and SF with only 25 objects (33.33%) being categorised as SNe Ia by all three classification tools - this forms a lower bound to the amount of SNe Ia actually found by the survey. The upper bound is the union of the three classification tools, where 61 objects (81.33%) in the survey are found to be classified as SNe Ia by at least one classification tool.

The proportions and the SNR analysis are combined to determine

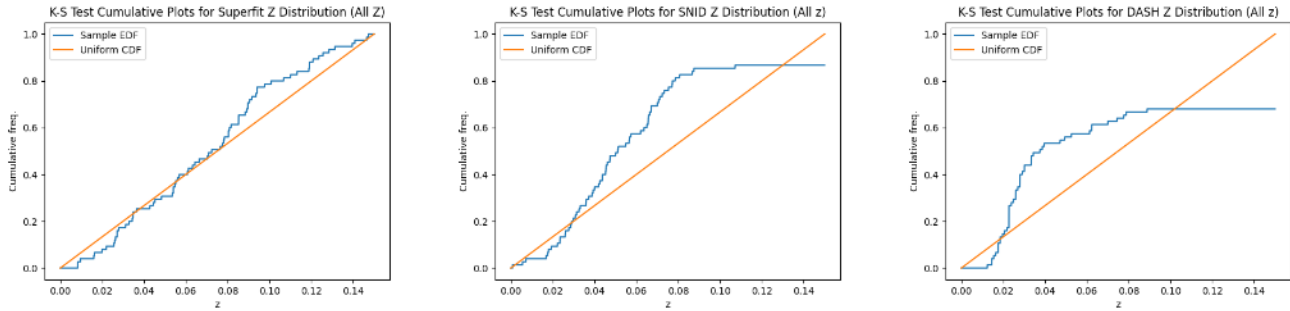


Figure 10. Plots of the empirical distribution function (EDF) of the SF (top), SNID (middle), and DASH (bottom) redshifts and the cumulative distribution function (CDF) of a uniform distribution. Both plots are required in determining a value for the K-S statistic. The EDFs additionally account for results in the entire redshift range.

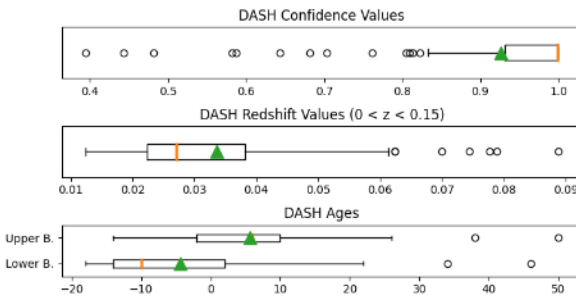


Figure 11. Boxplots of the confidence values (top), redshifts (middle) and upper & lower age ranges (bottom) obtained from the DASH program. Some objects were found to have a redshift greater than 0.15, they are not included as they plausibly cannot be in $z > 0.15$.

how much the presence of observable spectral features affected the classification of SNe Ia and Ia-norm. SF has an overlap of 64.44% with SNe Ia and $\text{SNR} > 5$, SNID has an overlap of 66.07%, and DASH has an overlap of 62.86%. When taking all three classification tools into account, only 11 objects (14.67%) have agreement on all three classification tools with SNRs greater than 5. 44 objects (58.67%) are classified by at least one tool as SNe Ia and has an SNR of greater than 5, making a 72.13% proportion from the other union type.

4 DISCUSSION

For the first two years, the survey has provided a substantial enough amount of data to analyse. However what must be determined is how much of this data is worth analysis. It is very likely that sizeable portions of the survey may not have a high enough SNR for spectral analysis or that the classification tools may not provide a satisfactory classification. It is important to not discard the report results but not to use it either as the be-all-end-all of the direction of future research.

What is also important to mention is how the data will be able to combine itself with other surveys, not only just the wider DEBASS project, but other surveys as well like LSST. [Bailey et al. \(2022\)](#) details the process of combining other sample data with the LSST deep field observations. This report will not focus to greatly on analysing the changes DEBASS will make to other SNe Ia surveys, particularly for use in dark energy estimation. As the source details, Euclid focused on wide and deep fields in the near-IR range rather

than low-redshift optical spectra. It is worthwhile to still mention such considerations.

In the past, SNe Ia surveys have been limited by temporal observation rather than SNR or sample size ([Parrent et al., 2014](#)). However with the use of the 2.3 m telescope and the apparent results of the survey, it is clear that sample size and SNR will affect the limitations of the survey - more so caused by more ambitious requirements of size and clarity due to the cosmological crisis.

The use of some methods may not provide the most insightful analysis as well, noting how the KS-tests involve the creation of EDFs, which can prevent correspondence analysis. The redshift distribution becomes untethered to the respective SNe, and thus the goodness-of-fit measure a KS-test provides is a superficial whole-survey look rather than matching redshift to corresponding redshift; KS-tests cannot account for a particular SNe Ia candidate being marked as $z = 0.04$ and $z = 0.12$ by two different tools. Correlation or discrete unit tests similar to Chi-Squared analysis may account for the lack of overlap accountability.

Both proportions and SNe Ia counts matter when making conclusions about the survey. While the amount of SNe Ia classified matters, this does not take into account future progression. Proportions can highlight what the survey may look like by the end, assuming that the same rates of random failure and success events are occurring. The scenario where all of the observed SNe Ia will stay the same in amount is unlikely, but the idea that all proportions will stay relatively the same makes a large assumption on the sampling rate and bias of the collected data including how it will go in the future.

4.1 Spectral Analysis

The signal-to-noise ratio is the window into obtaining spectral analysis. From the introduction, all of the desired spectral features to be analysed are: SiIII, CaII, NiII, [Mg/Fe], [α /Fe], [Fe/H], TiIII, Cri, FeI, [OII], OI, HeI, and Balmer emission. As stated prior, the most important features for both identifying the type and age of SNe Ia are Silicon and Nickel. Fortunately they require a lower SNR due to the broadness of lines, although Nickel appears more strongly in the B-band. The other spectral tools may require more quality and thus have a higher bar to meet. While SNR is not the only metric that needs to be taken into account when determining resolution, it provides some view into the quality of the data.

With a detectable SNR skewed towards the lower end, a large portion of the survey may be unable to have enough resolution to be able to make fair judgements on the spectral features of the SNe Ia

classification tools	Candidate Type	No. of Objects	Proportion of Set
SF	Ia-norm*	23	0.3067
	Ia-norm	35	0.4667
	Ia*	29	0.3867
	Ia	45	0.6
	Ib or Ic	22	0.2933
	Non-type I (type II)	17	0.2267
SNID	Ia-norm*	33	0.44
	Ia-norm	50	0.6667
	Ia*	37	0.4933
	Ia	56	0.7467
	Ib or Ic	6	0.08
	Non-type I (type II, M-Star, Galaxy)	13	0.1733
DASH	Ia-norm*	4	0.05333
	Ia-norm	5	0.0667
	Ia*	22	0.2933
	Ia	35	0.4667
	Ib or Ic	38	0.5067
	Non-type I (IIP, IIb)	2	0.0267
Human/Manual	Ia	45	0.6
SF & SNID (Int.)	Ia*	11	0.1466
	Ia	26	0.3467
SF & DASH (Int.)	Ia*	26	0.3467
	Ia	41	0.5467
SNID & DASH (Int.)	Ia*	18	0.24
	Ia	33	0.44
Union (At least 1 of SF, SNID, or DASH)	Ia*	44	0.5867
	Ia	61	0.8133
Intersection (All 3 of SF, SNID, and DASH)	Ia*	11	0.1467
	Ia	25	0.3333

Table 3. A table of all of the candidate types broken down by classification tool source, tallied up to determine both the amount and proportion of the data set they make up. The middle section displays human analysis. The bottom five rows display the intersections and unions of multiple analysis methods.

* Indicates that the data was first filtered for spectra with a R-band SNR of greater than 5.

candidates. This presents itself clearly with the inability of the three classification tools to be so certain of the spectral subtype - or even general type of the object. Only 33% of the survey are consistently classified as SNe Ia. However, this data is usable in the case of distance estimation, and potentially in age-based model training, as no particular lines need to be investigated to determine age (Hoeflich et al., 2017).

The presence of the skew is most likely due to environmental factors of observation that affect optical spectra, demonstrating the limitations thereof. Atmospheric conditions and distance can both affect the SNR, meaning that it is expected for higher SNR SNe Ia to be found at lower redshift. More resolute optical telescopes would be required for high-redshift optical observation of SNe Ia. Host galaxy conditions may cause the greatest amount of noise second to atmosphere. Given that a large amount of SNe Ia candidates were determined to be in early-phase spiral galaxies, the density of gas can certainly affect the observation of SNe Ia. However, this also provides greater opportunity to investigate the relationship between host galaxy environment and SNe Ia spectra as spectra 'clouded' by gas in their local environment can still be analysed - giving credence to SF's ability to take into account the galactic environment. Host galaxies will still allow for redshift classification. This is apparent in how SF is able to have a few low-SNR objects being classified as SNe Ia.

It is also important to note the differentiation and purpose of the 'uncut' and 'cut' SNR values. For a majority of the objects, the spectra has an incredibly low SNR in the B-band range, getting increasingly worse with decreasing wavelength. It is not likely that the B-band of any of the SNe Ia can be utilised for emission or absorption-based

spectral analysis. Thus it may be more useful to provide data in the form of a 'cut' spectra, only looking at the R-band which starts at 5300 Å. Performing the cutoff does have a noticeable effect on the SNRs of the survey as a whole, however the most it does is shift most SNRs up by a unit or so - keeping the same distribution and variance but with now a higher mean and median. R-Band SNRs are used and preferred throughout the remainder of the report.

From percentile analysis in 3, a fair three fifths of the survey still have SNRs of above 5. This minimum bound on the required spectral resolution implies that a large portion of the survey can still have Silicon and Nickel analysis conducted. Silicon, of course can allow a much clearer estimation of the rate of SNe Ia. From the proportionality results, it is clear that about 65-70% of whatever 'determined amount' of SNe Ia will have SNRs of greater than this minimum bound. Thus there is still a great potential for the current survey to provide age and redshift analysis reliably.

About two fifths of the survey have SNRs of above 10. This is the minimum bound set for metallicity analysis, and it implies that there is a good enough presence of data to perform at least a basic determination of α -metallicity or [Fe/H] metallicity. In reference to the metallicity section, Millán-Irigoyen et al. (2022); Ruiter (2019) references how metallicity can have a sizeable impact on the light curve evolution and formation of accurate Hubble diagrams. Thus having a decent amount of high-SNR spectra can be good for not only training models to account for this relationship, but also a more robust form of distance estimation.

With other spectral features, as one to two fifths of the survey contain spectra of high enough SNRs, it is possible to use those ob-

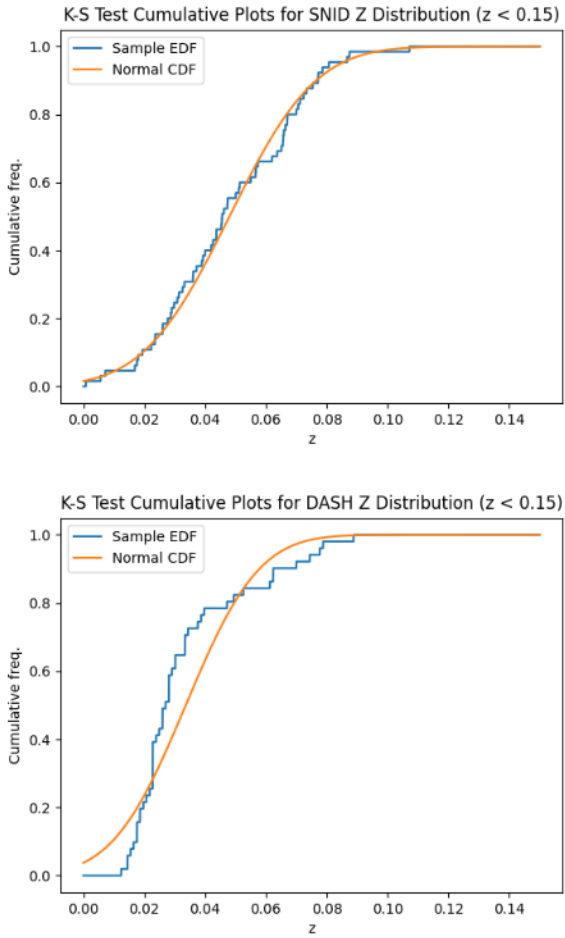


Figure 12. Plots of the empirical distribution function (EDF) of the SNID (top) and DASH (bottom) redshifts and the cumulative distribution function (CDF) of a normal distribution. The EDFs are restricted to the $0 < z < 0.15$ redshift range.

jects in future research on spectral analysis of SNe Ia. One fifth only amounts to 15 objects at the present moment, however, so there may be difficulty in combining this data with other surveys of different standardisation. Identifying each object on its own and then attempting to observe the optical spectra again but with a more resolute telescope may be useful. Either way, the survey still provides data that can be used for future investigation.

4.2 Sampling Bias and Methodological Comparison

There are several possible z-distributions that could be generated from analysis of the survey spectra. Ideally, a uniform distribution is desired. However from [Kessler et al. \(2019\)](#), it may be more likely to see a skew towards lower z-values. Taking into account the volumetric distribution of SNe Ia, it might be easier to see a power law with redshift of some form. With age, a normal distribution is expected that is centred around zero phase.

SF has a very cleanly uniform z-distribution, the most out of all the classification tools, while this is very promising, it would be falling into confirmation bias to prioritise SF simply because it gives a desired distribution. In fact, it may be less likely for the survey

to find such a cleanly uniform distribution. Other metrics about the program must be used to quantify the reliability and validity of SF first. The uniformity of the model can also be explained by the parameterised values. Unlike the other two models, SF is capable of remaining strictly within a specified redshift range for analysis - this potentially can 'compress' the data within to the desired range without concern for if it is reasonable to assume it can. This possible explanation is limited by the fact that a) it is known that all objects should be in the $0 < z < 0.15$ range (it may be worthwhile revisiting this assumption), and that b) this 'compression' of data does not necessarily mean it should produce a uniform distribution - after all, it could have produced, and would be expected to, produce a distribution that appears more like DASH's.

SNID appears as the most unusual in terms of z-distribution, with an incredibly high correspondence to a normal distribution. This implies that at some stage in the process of classification the central limit theorem came into effect where it did not in other surveys. Theoretically, there should be no normal distribution in redshift as there is no reason for data to accumulate towards a central value. A possible explanation for this is SNID's approach to analysis. The program follows along with a very 'throw everything at the wall and see what sticks' approach of trial and error. The repeated tests and trials over and over again may cause redshift values to centralise, producing a normal distribution.

DASH has a z-distribution that is partly normal, but unlike the strangeness that SNID produces, this distribution can be more easily explained. Figure 7 in the report by [Kessler et al. \(2019\)](#) demonstrates how the SALT-2 intrinsic scatter model will produce an expected low-z redshift distribution that is heavily skewed towards lower values of z. This implies that while there are significant apparent limitations in the DASH model, enough so to determine that it is the 'least' effective at classification, there is more to its analysis. Further research must be conducted to make sure that this distribution was not caused by pure chance.

There is a notable lack of robustness in the DASH program. Evidenced by the stark difference between the classification tool and the other two tools, in addition to the significant bias towards non type-Ia SNe, and the lack of classification of Ia-norm SNe. It is referenced in the report by [Muthukrishna et al. \(2019\)](#) that the AI models trained highlighted half their training data as Ia-norm, a major difference from the 5 objects classified by the tool using this survey. With the use of AI, there are many potential sensitivities to real-world data analysis that could cause this. As aforementioned, host galaxy environment can also play a role in the observation of spectral features, a highlighted quality of SF. However, DASH is also capable of host galaxy environment classification, despite it not being utilised in the development of analysed data points. This limitation imposed on DASH may have greatly affected its perceived performance. It is possible that due to the lack of host galaxy analysis, DASH was unable to use the AI effectively. AI reliant on neural networks may not be able to tell the difference between a host galaxy feature and an object feature. Additionally, the order of analysis may incorrectly determine the redshift, which can disturb the model's classification of spectra. This limitation does not appear for SNID primarily because SNID uses a trial-and-error approach, comparing an incredibly large amount of sample data to the spectra - this produces a very large amount of type-based analysis, as mentioned already potentially being the cause of its normal distribution.

With this, SF provides significant advantages and reliability due to its ability to classify SNe Ia and their respective host environment. The data presented in fig. 6 shows an expected classification that most SNe Ia reside in early-phase spiral galaxies. Unfortunately, due

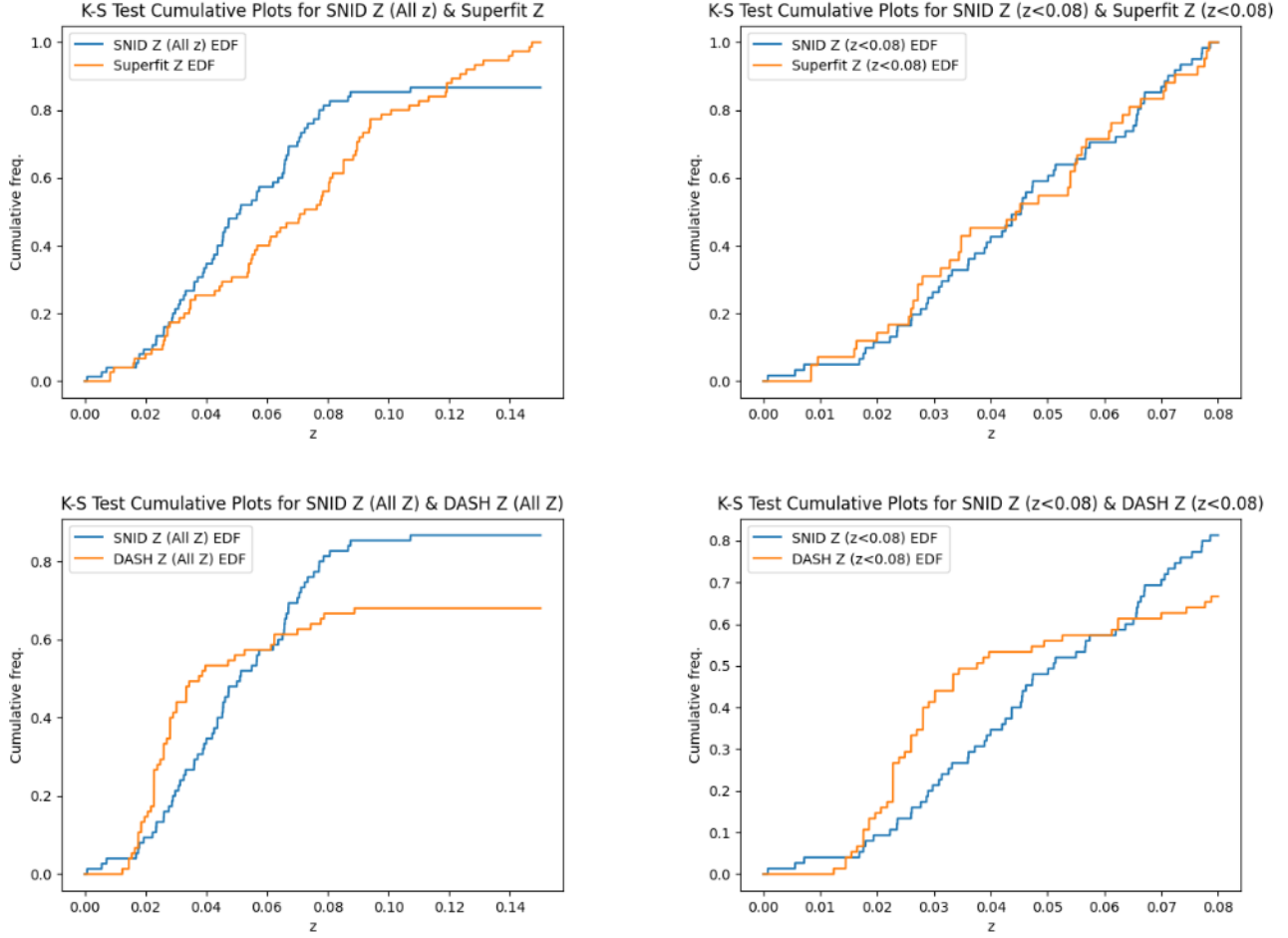


Figure 13. Plots of the empirical distribution functions of the redshift distributions of each of the three samples when compared with each other. The EDFs of SNID and SF z distributions compared together for all z (top left) and for $z < 0.08$ (top right). The EDFs of SNID and DASH are compared for all z (bottom left) and for $z < 0.08$ (bottom right).

to several limitations, SF could not classify Elliptical galaxies with more precision into the E0-E7 range. The analysis of these galactic subtypes would provide further insight onto the perceived accuracy of SF's analysis. It would be worthwhile to see if this classification works as well with DASH.

Mutual consensus is what is required to determine the proper redshift range. And given the comparison between distributions in fig. 13, especially focused on the $0 < z < 0.08$ range, SNID and SF appear to agree with each other more than SNID agrees with DASH. This can point to the potential that the results of DASH might be compromised and unreliable. This is contrasted with the results from table 3, which determines that SF and DASH agree more with each other than SF and SNID, highlighting a reliability in classification for DASH. Despite this, the use of KS-tests are prioritised over the proportionality analysis, primarily because the rate of classification for SF-SNID or SF-DASH are still relatively similar, whereas there is a significant difference in the overlap or lack thereof of the samples. And additionally DASH and SNID only appear to agree on a very low-data level when restricting to Ia-norm SNe Ia.

What all three models seem to agree the most on is age. From fig. 14 all models appear to follow a normal distribution centred at zero phase. This is expected, as all SNe Ia would be observed at around peak brightness. Again, SF appears the most uniform. This is most

likely due to limitations in the SF software to provide a definite age value. This uniformity does not appear to vanish when restricting to Ia-norm SNe. SNID and DASH appear to agree more. But because the KS-tests are limited at low sample sizes, the classification issues of DASH make it less able to provide a match with SNID. Overall, it appears that SNID is the most reliable at classifying age given its method. However this could also be another consequence of the central limit theorem with no direction to meaningful age classification.

4.3 Confidence Intervals and Overlap

Table 3 provides important details on the agreement between the different methods on a proportional classification basis rather than using the data points of redshift and age. It also allows for a corroboration between automated and manual analysis. From the table, it is clear that SNID might over-classify SNe Ia, as it presents a proportion that is too high compared to all of the other data points. The agreement between SNID and the other two methods additionally reduce the count to a significantly lower value. SF appears as the most mid-way point, with the closest correspondence to human analysis. DASH appears to under-classify SNe Ia, particularly due to how it over-classifies SNe Ib and Ic. The union and intersection fields of

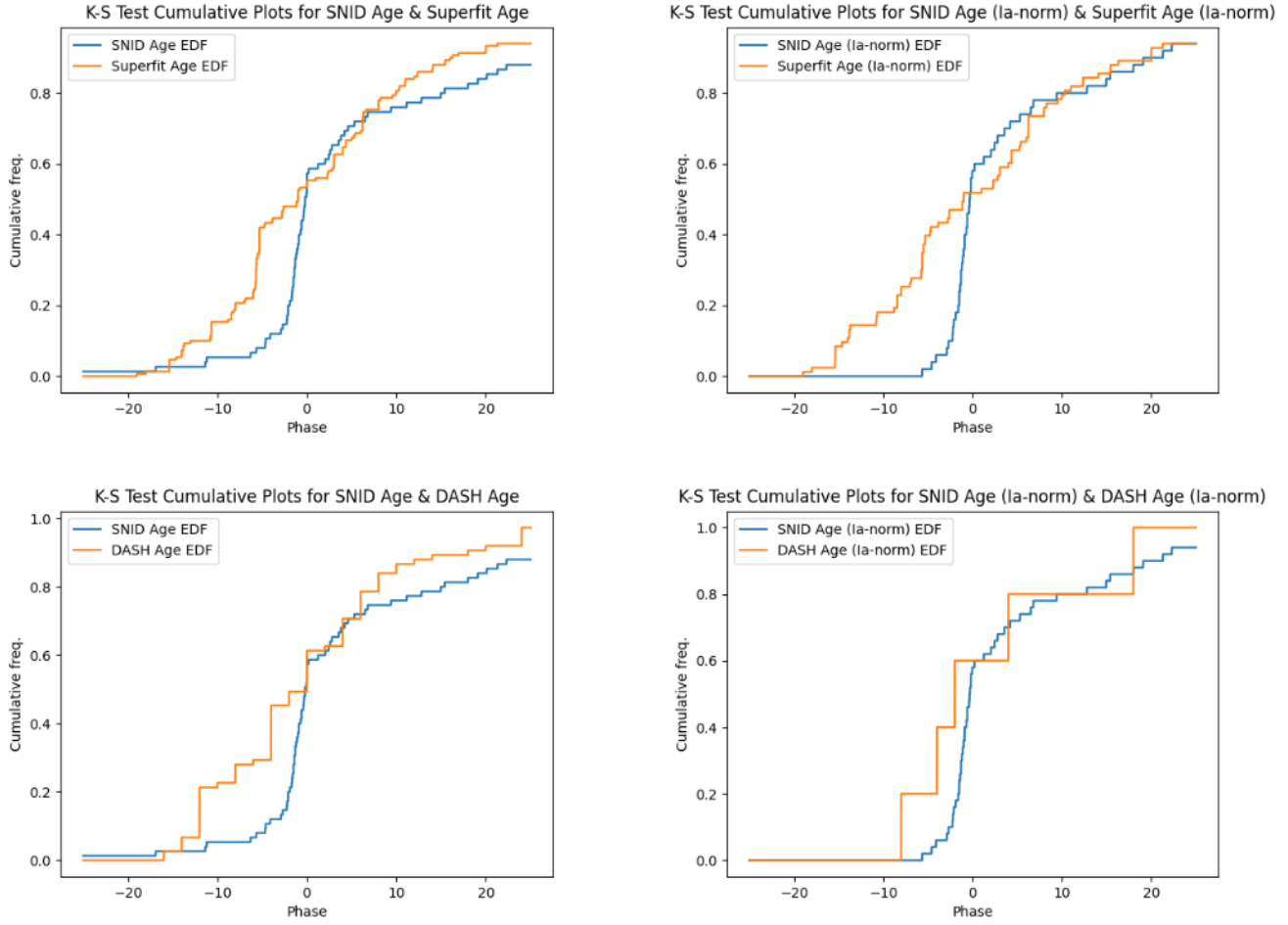


Figure 14. Plots of the empirical distribution functions of the age distributions of each of the three samples when compared with each other. The EDFs of SNID and SF age distributions compared together for all objects (top left) and restricted to Ia-norm SNe (top right). The EDFs of SNID and DASH are compared using the DASH average age metric for all objects (bottom left) and restricted to Ia-norm SNe (bottom right).

table 3 gives a proper upper and lower bound on the actual amount of SNe Ia. This places the survey proportion of SNe Ia between 33% and 81%.

This gives further credence to an estimated proportion value of 60%. As it aligns with both SF, human analysis, and falls within a reasonable 'middle value' between DASH, SNID, the union, and the intersection of classification tools. It also can reversibly demonstrate the reliability of SF in classifying SNe Ia in the correct amounts, appearing with no bias in non-SNe Ia classifications (which is not necessarily an expected result, but would be only if observation of non-SNe Ia is blind).

It is also implied from the SNR analysis that about 60% of the survey's SNe Ia successes have satisfactory SNR. This implies that 36% of the survey in total are both SNe Ia and have SNRs of above 5. The 64th percentile of SNR is 10.85 while the 40th percentile is 5.053. This demonstrates that while many of the survey objects are effectively unusable in regard to the two aims of the report, there is a fair amount of data, in equal size, that is use-able for all purposes.

A 60% collection rate also appears reasonable when considering the redshift overlap. About 44 objects (58.67%) consistently had redshift values within the range of $0 < z < 0.15$. This is very similar to other parts of the survey and shows that the classification tools

could all agree that 60% of the objects were in the desired low-z range.

4.4 Overall Survey Progression

Given a 60% collection rate of SNe Ia data corresponding to 45 of 75 objects, it is possible to determine the current direction that the project should go for its third or even fourth year. The desired 30 SNe Ia per quarter goal is well above what actually has been recorded. Despite this, it was expected that the survey would not attain this goal.

There are many factors that can, and have, affected the rate at which SNe Ia are observed. The most plain of them is that one cannot determine if an object is an SNe Ia without observing it first. Because of this, there is a high likelihood that the survey would encounter non-type Ia SNe. It may also be reasonable to assume that the survey would be biased towards type I SNe generally simply because of the lack of Hydrogen in their spectra. But without information on the discovery process, such an assumption may not be made. However the difference between the two approaches, blind or I-biased may give leeway between SF or DASH, as demonstrated prior. This discovery process could also be biased by simply seeing objects that, from a distance, appear as SNe Ia.

The classification rate might be an issue of manual versus automated analysis. While the 60% benchmark follows human estimation closely, human classification that determines an object to be SNe Ia may not be a reliable process, much less so for analysis of Ti lines e.g. If a computer were to be given that the object was an SNe Ia, or even given a redshift, then the accuracy of analysis would be significantly greater. There are clearly limitations to both approaches that reduces reliability and accuracy. With a computer model, a failure rate can be partly caused by an initial lack of accurate classification.

There are other factors that affect the rate, or speed of observation. This rate is not affected by the classification tools at all but instead out-of-control events such as weather, technical failures, time of year, coordinate determination, etc. These did significantly slow down the rate of data collection, given the location of the 2.3 m telescope. This does not immediately imply that more can not be done to observe quicker, but it does not imply that the progress is due to poor performance.

Overall, a desired 250 SNe Ia spectra was to be obtained. The total size of the survey is 75, and about 45 objects so far are likely to be SNe Ia. This definitely is under the desired goal, however is a somewhat minor indicator of progress. DEBASS's third year would have to be busy in order to partly make up for the slow progress, and even a fourth year might be a good idea. Though the longer DEBASS runs for, the harder it may be to combine itself with future dark-energy estimation projects like the LSST.

5 CONCLUSIONS

The aim of the survey is two fold: a primary goal of gathering data for model training and dark energy distance estimation, and a secondary goal of providing more data for further spectral analysis of SNe Ia to determine their various properties. These two goals may complement each other via how the variations in SNe Ia can help further inform models using SNe Ia to estimate distance etc. Fulfilling the primary goal is a much more simple task, as obtaining a good redshift range and data variety is the core aim of the survey, whereas it is not expected that the survey would provide an incredible level of information to support the secondary goal.

From the analysis of proportionality, it is reasonable to say that 60% of the survey so far are SNe Ia. Making 45 objects in total that are most likely SNe Ia. Of course when establishing correlation relations, the more the better, and there is certainly a noticeable lack of SNe Ia two years into the project compared to the desired 200-300. However it is more likely that the goal set did not account for environmental factors. With the 60% benchmark, it appears that the SNe Ia candidates have a SNR of 5.1 and above. At the very least, this means that most of the SNe have measurable Ni and Si proportions, which will certainly help with age-based model training.

Despite the skew, a fair amount of data points in the survey have

SNR values that are above required minimums for analysis. 15 objects have SNR ratios well above what is required for detailed spectral analysis, and 29 objects are capable for metallicity, SiII, and NiII analysis - along with some other elements. There is almost a guarantee that some of these SN Ia have unique subtypes and spectral features that may provide useful for further research. However generally, if future reports were to utilise DEBASS data, there may be difficulty in combining the small handful of these objects with larger surveys.

With this in mind, the survey in its current progress appears on track to provide a spectroscopic complement for model training and dark energy, however a faster rate of candidate observation would be desirable - a rate which cannot necessarily be achieved given the factors that affect said observation rate. This is less so true for the secondary aim of the survey, providing a minor amount of potentially useful data for future research to investigate.

The survey also highlighted notable biases or behaviours in the modelling programs. While not enough analysis was performed and not enough data was present to make solid conclusions, the report still can highlight potential directions for future research and properties of the classification tools. SF appears to be the 'best' out of all three tools: its lack of overestimation and underestimation; the potential alignment with human analysis; its heavily parameterised model fitting; the ability to classify host galaxies; the provided chi-squared analysis. SNID works to a decent degree primarily because of the speed and trial-and-error style approach. Unlike the other two, DASH seems to lack the qualities required for good analysis, especially being unable to specify subtype and its bias towards non-Ia SNe. However it is important to note that its skew follows external modelling, and that there is always the potential for better classification if host galaxy classification can be conducted. Based on this report it is not worthwhile to discard any of the three tools, despite the apparent advantages and disadvantages. The mutual consensus created by applying multiple classification tools can help aid the certainty in classification, especially if classifications align better.

While proportions alone are not capable of determining overlap between the three data sets, with corroboration from the KS-tests, a decent estimate for survey overlap can be determined. Future analysis should involve fixing this issue of overlap, as it may point out more proper disagreement between the classification tools. This may alter the mutual consensus approach applied by the report.

ACKNOWLEDGEMENTS

We would like to thank A/Prof. Chris Lidman for making the observations and reductions of the SNe Ia candidate spectra, Patrick Armstrong for guidance on the compilation of the SNID/SuperFit/DASH programs in a manner that would be useful for future DEBASS research. The ANU DEBASS project can be accessed at <https://www.mso.anu.edu.au/debass>.

REFERENCES

- I. Acharova, M. E. Sharina, & E. A. Kazakov. (2022). Investigation of the prompt snc ia progenitor nature through the analysis of the chemical composition of globular clusters and circumgalactic clouds. *Monthly Notices of the Royal Astronomical Society*, 511(1), 800–813.
<https://arxiv.org/abs/2201.06481>
- A. Bailey, M. Vincenzi, D. Scolnic, et al. (2022). Type ia supernova cosmology combining data from the euclid mission and the vera c. rabin observatory. *arXiv*.
<https://arxiv.org/abs/2211.01206>
- M. Betoule, R. Kessler, J. Guy, et al. (2014). Improved cosmological constraints from a joint analysis of the sdss-ii and snls supernova samples. *Astronomy and Astrophysics*, 568, A22.
<https://www.aanda.org/articles/aa/abs/2014/08/aa23413-14/aa23413-14.html>
- S. Blondin, & J. L. Tonry. (2007). Determining the type, redshift, and age of a supernova spectrum. *The Astrophysical Journal*, 666(2), 1024–1047.
<https://arxiv.org/abs/0709.4488v1>
- E. Bravo, L. Piersanti, S. Blondin, et al. (2022). Chandrasekhar-mass white dwarfs are the progenitors of a small fraction of Type Ia supernovae according to nucleosynthesis constraints. *Monthly Notices of the Royal Astronomical Society: Letters*, 517(1), L31–L35.
<https://doi.org/10.1093/mnrasl/slac103>
- X. Chen, L. Wang, L. Hu, et al. (2022). Artificial intelligence assisted inversion (aiai): Quantifying the spectral features of 56ni of type ia supernovae. *arXiv*.
<https://arxiv.org/abs/2210.15892>
- R. C. V. Coelho, M. O. Calvão, R. R. R. Reis, et al. (2014). Standardization of type ia supernovae. *The Astrophysics Journal*, 36(1), 015007.
<https://iopscience.iop.org/article/10.1088/0143-0807/36/1/015007>
- C. E. Collins, S. Gronow, S. A. Sim, et al. (2022). Double detonations: variations in type ia supernovae due to different core and he shell masses - ii. synthetic observables. *Monthly Notices of the Royal Astronomical Society*, 517(4), 5289–5302.
<https://academic.oup.com/mnras/article/517/4/5289/6713959>
- E. di Valentino, O. Mena, S. Pan, et al. (2021). In the realm of the hubble tension—a review of solutions*. *Classical and Quantum Gravity*, 38(15), 153001.
<https://dx.doi.org/10.1088/1361-6382/ac086d>
- M. Dixon, C. Lidman, J. Mould, et al. (2022). Using host galaxy spectroscopy to explore systematics in the standardization of type ia supernovae. *Monthly Notices of the Royal Astronomical Society*, 517(3), 4291–4304.
<https://academic.oup.com/mnras/article/517/3/4291/6764741>
- M. Dopita, J. Hart, P. McGregor, et al. (2007). The wide field spectrograph (WiFeS). *Astrophysics and Space Science*, 310(3-4), 255–268.
<https://doi.org/10.1007%2Fs10509-007-9510-z>
- A. V. FILIPPENKO. (1989). Type ia supernovae in elliptical and spiral galaxies: Possible differences in photometric homogeneity. *Publications of the Astronomical Society of the Pacific*, 101(640), 588–593.
<http://www.jstor.org/stable/40679363>
- A. V. Filippenko. (1997). Optical spectra of supernovae. *Annual Review of Astronomy and Astrophysics*, 35, 309–355.
- A. V. Filippenko, & A. G. Riess. (1999). Type ia supernovae and their cosmological implications. *arXiv*.
<https://arxiv.org/abs/astro-ph/9905049>
- R. J. Foley, D. Scolnic, A. Rest, et al. (2017). The foundation supernova survey: Motivation, design, implementation, and first data release. *Monthly Notices of the Royal Astronomical Society*, 475(1), 193–219.
<https://arxiv.org/abs/1711.02474>
- P. J. Gandhi, A. Wetzel, P. F. Hopkins, et al. (2022). Exploring metallicity-dependent rates of type ia supernovae and their impact on galaxy formation. *Monthly Notices of the Royal Astronomical Society*, 516(2), 1941–1958.
<https://academic.oup.com/mnras/article/516/2/1941/6660657>
- P. Gris, N. Regnault, H. Awan, et al. (2023). Designing an optimal lsst deep drilling program for cosmology with type ia supernovae. *The Astrophysics Journal*, 264(1), 22.
<https://iopscience.iop.org/article/10.3847/1538-4365/ac9e58>
- R. R. Gupta. (2013). Understanding Type Ia Supernovae Through Their Host Galaxies Using the SDSS-II Supernova Survey. *Publicly Accessible Penn Dissertations*, (758).
<https://repository.upenn.edu/edissertations/758>
- J. Guy, P. Astier, S. Baumont, et al. (2007). Salt2: using distant supernovae to improve the use of type ia supernovae as distance indicators. *Astronomy and Astrophysics*, 446(1), 11–21.
<https://www.aanda.org/articles/aa/abs/2007/16/aa6930-06/aa6930-06.html>
- P. Hoeflich, E. Y. Hsiao, C. Ashall, et al. (2017). Light and color curve properties of type ia supernovae: Theory versus observations. *The Astrophysical Journal*, 846(1), 58.
<https://dx.doi.org/10.3847/1538-4357/aa84b2>
- D. A. Howell, M. Sullivan, K. Perrett, et al. (2005). Gemini spectroscopy of supernovae from snls: Improving high redshift sn selection and classification. *The Astrophysical Journal*, 634(2), 1190–1201.
<https://arxiv.org/abs/astro-ph/0509195v1>
- J. Johansson, S. B. Cenko, O. D. Fox, et al. (2021). Near-infrared supernova ia distances: Host galaxy extinction and mass-step corrections revisited. *The Astrophysics Journal*, 923(2), 237.
<https://iopscience.iop.org/article/10.3847/1538-4357/ac2f9e>
- L. Kelsey, M. Sullivan, M. Smith, et al. (2020). The effect of environment on type ia supernovae in the dark energy survey three-year cosmological sample. *Monthly Notices of the Royal Astronomical Society*, 501(4), 4861–4876.
<https://academic.oup.com/mnras/article/501/4/4861/6043221>
- L. Kelsey, M. Sullivan, P. Wiseman, et al. (2022). Concerning colour: The effect of environment on type ia supernova colour in the dark energy survey. *Monthly Notices of the Royal Astronomical Society*, 519(2), 3046–3063.
<https://academic.oup.com/mnras/article/519/2/3046/6939845>
- R. Kessler, D. Brout, C. B. D'Andrea, et al. (2019). First cosmology results using type ia supernova from the dark energy survey: simulations to correct supernova distance biases. *Monthly Notices of the Royal Astronomical Society*, 485(1), 1171–1187.
<https://doi.org/10.1093%2Fmnras%2Fstz463>
- A. Kim, N. Padmanabhan, G. Aldering, et al. (2015). Distance probes of dark energy. *Astroparticle Physics*, 63, 2–22. Dark Energy and CMB.
<https://www.sciencedirect.com/science/article/pii/S0927650514000772>
- C. Liu, A. A. Miller, A. Polin, et al. (2022). Sn 2020jgb: A peculiar type ia supernova triggered by a massive helium-shell detonation in a star-forming galaxy. *arXiv*.
<https://arxiv.org/abs/2209.04463>
- E. Macaulay, R. C. Nichol, D. Bacon, et al. (2019). First cosmological results using type ia supernovae from the dark energy survey: measurement of the hubble constant. *Monthly Notices of the Royal Astronomical Society*, 486(2), 2184–2196.
<https://academic.oup.com/mnras/article/486/2/2184/5435505>
- K. Maeda, & M. Kawabata. (2022). Properties of type iax supernova 2019muj in the late phase: Existence, nature, and origin of the iron-rich dense core. *The Astrophysics Journal*, 941(1), 15.
<https://iopscience.iop.org/article/10.3847/1538-4357/ac9df2>
- F. Mannucci, M. Della Valle, N. Panagia, et al. (2005). The supernova rate per unit mass. *Astronomy & Astrophysics*, 433(3), 807–814.
- C. Meldorf, A. Palmese, D. Brout, et al. (2022). The dark energy survey supernova program results: type ia supernova brightness correlates with host galaxy dust. *Monthly Notices of the Royal Astronomical Society*,

- 518(2), 1985–2004.
<https://academic.oup.com/mnras/article/518/2/1985/6775122>
- X.-C. Meng, J.-J. Zhang, X. Zhao, et al. (2023). Environments of type ia supernovae with different relative equivalent widths of the si ii feature in their spectra. *The Astrophysics Journal*, 943(2), 159.
<https://iopscience.iop.org/article/10.3847/1538-4357/acad77>
- B. J. Miles, D. R. van Rossum, D. M. Townsley, et al. (2016). On measuring the metallicity of a type ia supernova's progenitor. *The Astrophysics Journal*, 824(1), 59.
<https://iopscience.iop.org/article/10.3847/0004-637X/824/1/59>
- I. Millán-Irigoyen, M. G. del Valle Espinosa, R. Fernández-Aranda, et al. (2022). Stellar populations in type ia supernova host galaxies at intermediate-high redshift: Star formation and metallicity enrichment histories. *Monthly Notices of the Royal Astronomical Society*, 517(3), 3312–3331.
<https://academic.oup.com/mnras/article/517/3/3312/6712723>
- D. Muthukrishna, D. Parkinson, & B. E. Tucker. (2019). Dash: Deep learning for the automated spectral classification of supernovae and their hosts. *The Astrophysical Journal*, 885(1), 85.
<https://arxiv.org/abs/1903.02557>
- N. Nicolas, M. Rigault, Y. Copin, et al. (2021). Redshift evolution of the underlying type ia supernova stretch distribution. *Astronomy and Astrophysics*, 649, A74.
https://www.aanda.org/articles/aa/full_html/2021/05/aa38447-20/aa38447-20.html
- J. Parrent, B. Friesen, & M. Parthasarathy. (2014). A review of type ia supernova spectra. *Astrophysics and Space Science*, 351, 1–52.
<https://link.springer.com/article/10.1007/s10509-014-1830-1>
- S. Perlmutter, G. Aldering, G. Goldhaber, et al. (1999). Measurements of Ω and Λ from 42 High-Redshift Supernovae. *The Astrophysical Journal*, 517(2), 565–586.
- A. G. Riess, A. V. Filippenko, P. Challis, et al. (1998). Observational Evidence from Supernovae for an Accelerating Universe and a Cosmological Constant. *The Astrophysical Journal*, 116(3), 1009–1038.
- A. J. Ruiter. (2019). Type ia supernova sub-classes and progenitor origin. *Proceedings of the International Astronomical Union*, 15(S357), 1–15.
<https://arxiv.org/abs/2001.02947v2>
- P. Shah, P. Lemos, & O. Lahav. (2023). The impact of weak lensing on type ia supernovae luminosity distances. *Monthly Notices of the Royal Astronomical Society*, 520(1), L68–L71.
<https://academic.oup.com/mnrasl/article/520/1/L68/6998565>
- Y. Sharma, J. Sollerman, C. Fremling, et al. (2023). A systematic study of ia-csm supernovae from the ztf bright transient survey. *arXiv*.
<https://arxiv.org/abs/2301.04637>
- N. Smirnov. (1948). Table for estimating the goodness of fit of empirical distributions. *The Annals of Mathematical Statistics*, 19(2), 279–281.
<http://www.jstor.org/stable/2236278>
- M. Sullivan, D. Le Borgne, C. J. Pritchett, et al. (2006). Rates and Properties of Type Ia Supernovae as a Function of Mass and Star Formation in Their Host Galaxies. *The Astrophysical Journal*, 648(2), 868–883.
- G. Taylor, C. Lidman, B. E. Tucker, et al. (2021). A revised salt2 surface for fitting type ia supernova light curves. *Monthly Notices of the Royal Astronomical Society*, 504(3), 4111–4122.
<https://academic.oup.com/mnras/article/504/3/4111/6225808>
- M. Toy, P. Wiseman, M. Sullivan, et al. (2023). Rates and properties of type ia supernovae in galaxy clusters within the dark energy survey. *arXiv*.
<https://arxiv.org/abs/2302.05184>
- L. Verde, J. L. Bernal, A. F. Heavens, et al. (2017). The length of the low-redshift standard ruler. *Monthly Notices of the Royal Astronomical Society*, 467(1), 731–736.
<https://doi.org/10.1093/mnras/stx116>
- M. Vincenzi, M. Sullivan, A. Möller, et al. (2022). The dark energy survey supernova program: cosmological biases from supernova photometric classification. *Monthly Notices of the Royal Astronomical Society*, 518(1), 1106–1127.
<https://academic.oup.com/mnras/article/518/1/1106/6601453>
- D. O. Wells, S. L. Blatt, & W. E. Meyerhof. (1963). Decay of ni⁵⁶. *Phys. Rev.*, 130, 1961–1970.
<https://link.aps.org/doi/10.1103/PhysRev.130.1961>
- K. D. Wilk, D. J. Hillier, & L. Dessart. (2020). Understanding nebular spectra of type ia supernovae. *Monthly Notices of the Royal Astronomical Society*, 494(2), 2221–2235.
<https://academic.oup.com/mnras/article/494/2/2221/5801036>
- Y. Zenati, H. B. Perets, L. Dessart, et al. (2023). The origins of calcium-rich supernovae from disruptions of co white dwarfs by hybrid he–co white dwarfs. *The Astrophysics Journal*, 944(1), 22.
<https://iopscience.iop.org/article/10.3847/1538-4357/acaf65>

APPENDIX A: CHI-SQUARED WEIGHTED MODE ANALYSIS CONSTRUCTED IN PYTHON

```

import numpy as np

# Params: arr; an array of discrete or qualitative data
#          values.
# Params: chi2; an array with a one-to-one correspondence
#          with arr, containing the corresponding
#          chi-squared values.
# Returns: If unimodal, return the mode and the
#          confidence that said value is the mode.
#          If multi-modal, return the
#          mode-confidence with pair with the
#          highest confidence in that mode.
#
def chi2_weighted_mode(arr, chi2):
    # Get the counts for each value as normal
    vals, counts = np.unique(arr, return_counts=True)

    # Get a zipped list
    ziplist = list(zip(arr, chi2))

    # Calculate a weighted mode, where the weights
    # are the chi-squared values.

```

```

# Multiply each count by the average chi-squared
# of the value
chi2s = list(map(
    lambda x: np.mean(list(map(
        lambda y: y[1],
        filter(lambda y: x == y[0], ziplist)
    ))),
    vals
))

# Divide by chi-2 as bigger = badder
new_counts = [a/b for a,b in zip(counts, chi2s)]

index = np.argmax(new_counts)

return (
    vals[index],
    new_counts[index]/np.sum(new_counts)
)

```

This paper has been typeset from a $\text{\TeX}/\text{\LaTeX}$ file prepared by the author.